

Alternative “Bases” for Gradient-Based Optimization of Parameterized FM Radar Waveforms

Bahozhoni White, Matthew Heintzleman, Shannon D. Blunt
Radar Systems Lab (RSL), University of Kansas, Lawrence, KS

Abstract—Even for a fixed time-bandwidth product there are infinite possible spectrally-shaped random FM (RFM) waveforms one could generate due to their being phase-continuous. Moreover, certain RFM classes rely on an imposed basis-like structure scaled by underlying parameters that can be optimized (e.g. gradient-descent and greedy search have been demonstrated). Because these structures must include oversampling with respect to 3-dB bandwidth to account for sufficient spectral roll-off (necessary to be physically realizable in hardware), they are not true bases (i.e. not square). Therefore, any individual structure cannot represent all possible waveforms, with the waveforms generated by a given structure tending to possess similar attributes. Here we examine these attributes for some particular design structures, which may inform their selection for given radar applications.

Keywords—radar waveform design, waveform diversity, noise radar

I. INTRODUCTION

Radar waveform design has been a subject of significant attention for decades, with the emergence of arbitrary waveform generation (AWG) platforms combined with high-performance computing and optimization capabilities opening the door to a tremendous diversity of possibilities [1]. Waveforms possessing random attributes (e.g. noise radar [2,3]) is a prime example of these expanding prospects, where the particular class denoted as FM noise or random FM (RFM) [4-6] represents of subset thereof that is also amenable to high-power transmitters since such waveforms (being FM) are intrinsically constant amplitude and phase-continuous.

Spectrally-shaped versions of RFM [7] have been experimentally demonstrated to achieve lower range sidelobes and improved spectral containment, and thus less transmitter distortion. While a growing variety exists, the particular subclass relying on a parameterized structure has been recently shown [8] to be optimizable using gradient-descent in a manner based on fast Fourier transforms (FFTs), thereby enabling efficient design, and potentially facilitating a wide array of possible joint design considerations.

It is interesting to note that the basis-like structure used in [8] provides a means to optimize FM waveforms, yet does not make it possible to realize all possible FM signals since the imposed structure is not a true basis due to the practical need to account for oversampling. This requirement is critical in order to produce physically meaningful waveforms (see [9]), and therefore also suggests that alternative basis-like structures (e.g. Legendre polynomials [10]) could realize types of RFM signals possessing different characteristics. Moreover, it is important to note that this effect is a general consequence of designing

according to a physically meaningful basis-like structure and arises regardless of the particular optimization approach (i.e. not just the gradient-descent method in [8]).

To further explore the infinite space of waveform design structures, here we explore cases that naturally arise from ongoing work. Specifically, the 1st order polyphase-coded FM (PCFM) structure examined for gradient-descent optimization in [8] was also shown in [11] to be extensible to higher orders having different properties. We therefore investigate the impact of the 2nd order PCFM structure. The constant-envelope OFDM (CE-OFDM) construction from communications, and variants thereof, has also received growing attention as a possible avenue to produce new radar waveforms (e.g. [12-17]), and is considered here as well.

II. GRADIENT-BASED OPTIMIZATION OF FM WAVEFORMS

It was recently shown [8] that PCFM radar waveforms can be optimized using gradient-descent. A key attribute involves representing the parameterized 1st order PCFM waveform

$$s(t; \mathbf{x}) = \exp \left\{ j \left(\int_0^t g(\tau) * \left[\sum_{n=1}^N \alpha_n \delta(t - (n-1)T_1 \right] d\tau \right) \right\} \quad (1)$$

$$= \exp(j\phi(t; \mathbf{x})),$$

where $\phi(t)$ is the ensuing continuous phase function, and with $*$ denoting convolution between shaping filter $g(t)$ and a train of N impulses separated by T_1 that are weighted by parameters $\mathbf{x} = [\alpha_1 \alpha_2 \dots \alpha_N]^T$, for transpose operation $(\cdot)^T$. Discretization of (1) takes the form

$$\mathbf{s} = \exp(j\mathbf{B}\mathbf{x}), \quad (2)$$

where \mathbf{B} is an $M \times N$ “quasi-basis” matrix where $M \gg N$. This latter requirement addresses the need to oversample the discretized signal relative to 3-dB bandwidth so that sufficient spectral roll-off is captured (depends on degree of spectral containment) to limit transmitter distortion effects. The actual columns of \mathbf{B} are obtained by evaluating the integration in (1), in which the n th column is a discretization of

$$b_n(t) = \int_0^t g(\tau - (n-1)T_1) d\tau. \quad (3)$$

Given the discretized FM representation from (2), we can write the corresponding waveform autocorrelation as

$$\mathbf{r} = \mathbf{A}^H [(\mathbf{A}\bar{\mathbf{s}}) \odot (\mathbf{A}\bar{\mathbf{s}})^*], \quad (4)$$

with (2) zero-padded to form $(2M - 1)$ vector $\bar{\mathbf{s}} = [\mathbf{s}^T \mathbf{0}_{1 \times (M-1)}]^T$. Here, \odot , $(\cdot)^*$, and $(\cdot)^H$ denote the Hadamard product,

complex-conjugate, and Hermitian operations, respectively, and with \mathbf{A} and \mathbf{A}^H the discrete Fourier transform (DFT) and inverse DFT, respectively. Per [8], the p -norm-based generalized integrated sidelobe level (GISL) metric is

$$J_p = \frac{\|\mathbf{w}_{\text{SL}} \odot \mathbf{r}\|_p^2}{\|\mathbf{w}_{\text{ML}} \odot \mathbf{r}\|_p^2}, \quad (5)$$

where \mathbf{w}_{ML} and \mathbf{w}_{SL} are length $(2M-1)$ vectors that respectively select the mainlobe and sidelobe regions of \mathbf{r} . The ensuing gradient of (5) with respect to the parameters in \mathbf{x} is then [8]

$$\nabla_{\mathbf{x}} J_p = 4J_p \bar{\mathbf{B}}^T \times \Im \left\{ \bar{\mathbf{s}}^* \odot \left(\mathbf{A}^H \left[\mathbf{A} \left(\left[\frac{\mathbf{w}_{\text{SL}}}{\mathbf{w}_{\text{SL}}^T |\mathbf{r}|^p} - \frac{\mathbf{w}_{\text{ML}}}{\mathbf{w}_{\text{ML}}^T |\mathbf{r}|^p} \right] \odot |\mathbf{r}|^{(p-2)} \odot \mathbf{r} \right) \odot (\mathbf{A} \bar{\mathbf{s}}) \right] \right) \right\} \quad (6)$$

with $\Im\{\cdot\}$ extracting the imaginary part of the argument. The result in (6) is employed in the gradient-descent implementation

$$\mathbf{x}_i = \mathbf{x}_{i-1} + \mu_i \mathbf{q}_i, \quad (7)$$

whereby

$$\mathbf{q}_i = \begin{cases} -\nabla_{\mathbf{x}} J_p(\mathbf{x}_{i-1}) & \text{when } i = 0 \\ -\nabla_{\mathbf{x}} J_p(\mathbf{x}_{i-1}) + \beta \mathbf{q}_{i-1} & \text{otherwise.} \end{cases} \quad (8)$$

Here, μ_i is the step-size for the i th iteration, $0 < \beta < 1$ is a ‘‘heavy ball’’ gradient-descent parameter [18], and

$$\bar{\mathbf{B}} = \left[\mathbf{B}^T \mathbf{0}_{N \times (M-1)} \right]^T \quad (9)$$

zero-pads the quasi-basis to agree with the zero-padding in $\bar{\mathbf{s}}$.

In [8] this approach was shown to produce a variety of different physically realizable waveform types depending on the specific p -norm value and the initialization of \mathbf{x} . For instance, higher p produced flatter sidelobes. Of course, while the 1st order quasi-basis from (3) is a logical outcome since it arises from continuous phase modulation (CPM) [19], from a mathematical standpoint \mathbf{B} is arbitrary. As long as the columns of \mathbf{B} possess sufficient oversampling to adequately capture spectral roll-off outside the 3-dB bandwidth (noting that a pulsed signal cannot be bandlimited and thus some aliasing is unavoidable), then a given instantiation is valid. Indeed, the cost function (5) and gradient-descent optimization approach from [8] are likewise arbitrary from this basis-like perspective.

In general, there are an infinite number of FM waveform possibilities since the instantaneous phase trajectory is a continuum. To establish some of the distinct attributes that arise, here we examine two additional quasi-bases in particular. Specifically, the 2nd order PCFM model developed in [11] allows for an exact representation of the linear FM (LFM) waveform – the above 1st order PCFM can only approximate LFM – suggesting smoother continuous phase functions may be obtained. We also consider the Fourier quasi-basis from the CE-OFDM structure, which has been shown to provide a natural degree of spectral containment for random

instantiations [12-15]. Note that the latter approach is also concurrently explored in [20].

III. 2ND-ORDER PCFM REPRESENTATION

It is shown in [11] that the 2nd order PCFM continuous phase function can be written as

$$\phi_2(t; \mathbf{x}_2) = \bar{\omega}_2 t + \iint_{0 \ 0}^t \tau \chi_2(\tau'; \mathbf{x}_2) d\tau' d\tau, \quad (10)$$

where $\bar{\omega}_2$ is the initial frequency and the coded instantaneous chirp rate is

$$\chi_2(t; \mathbf{x}_2) = \sum_{n=1}^N \alpha_{2,n} g_2(t - (n-1)T_1). \quad (11)$$

Here $g_2(t)$ is the 2nd order shaping filter and the 2nd order parameters are $\mathbf{x}_2 = [\alpha_{2,1} \ \alpha_{2,2} \ \dots \ \alpha_{2,N}]^T$. Selecting the former to be a rectangular filter with time support on $[0, T_1]$, which is the same as used for 1st order PCFM, results in the n th quasi-basis function being an oversampled discretization of

$$b_{2,n}(t) = \iint_{0 \ 0}^t g_2(\tau' - (n-1)T_1) d\tau' d\tau = \begin{cases} 0, & 0 \leq t < (n-1)T_1 \\ t^2/(2T_1^2) - (n-1)t/T_1 + (n-1)^2/2, & (n-1)T_1 \leq t < nT_1 \\ t/T_1 + 1/2 - n, & nT_1 \leq t \leq NT_1 \end{cases} \quad (12)$$

in which the center and bottom lines are a quadratic and a linear ramp, respectively.

Where 1st order PCFM has continuous phase, but involves discontinuous instantaneous frequency, the 2nd order version is continuous in both phase and frequency by virtue of the double integral. Consequently, proper choice of parameterization is expected to lead to better spectral containment (and thus greater utility when strict containment is critical). Indeed, this form can exactly produce an LFM waveform by choosing $\alpha_{2,n} = 2\pi/N$ for all n , which has very tight containment.

The instantaneous frequency for 2nd order PCFM can be readily shown by taking the derivative of (10), yielding

$$\omega_2(t; \mathbf{x}_2) = \frac{d}{dt} \phi_2(t; \mathbf{x}_2) = \bar{\omega}_2 + \sum_{n=1}^N \alpha_{2,n} \frac{d}{dt} b_{2,n}(t), \quad (13)$$

in which

$$\frac{d}{dt} b_{2,n}(t) = \begin{cases} 0, & 0 \leq t < (n-1)T_1 \\ t/T_1^2 - (n-1)/T_1, & (n-1)T_1 \leq t < nT_1 \\ 1/T_1, & nT_1 \leq t \leq NT_1 \end{cases} \quad (14)$$

reveals a linear frequency change over each continuous-time interval $(n-1)T_1 \leq t \leq nT_1$. In other words, the instantaneous frequency function is piece-wise linear for 2nd order PCFM.

Now discretize the n th quasi-basis function to obtain \mathbf{b}_n and in the same manner denote \mathbf{t} as the discretization of continuous time. Consequently, (10)-(12) can be expressed in discrete form

$$\mathbf{s}_2 = \exp(j\mathbf{B}_2 \tilde{\mathbf{x}}_2), \quad (15)$$

for $M \times (N+1)$ quasi-basis matrix $\mathbf{B}_2 = [\mathbf{b}_1 \ \mathbf{b}_2 \ \dots \ \mathbf{b}_N \ \mathbf{t}]$ and length $(N+1)$ parameter vector $\tilde{\mathbf{x}}_2 = [\mathbf{x}_2^T \ \bar{\omega}_2]^T$. In general, it is necessary to include the initial frequency term as one of the

optimizable parameters because it serves to keep the aggregate spectrum centered at zero (at baseband).

IV. FOURIER-BASED REPRESENTATION

The Fourier-based representation is the same as the CE-OFDM signal model, though we specifically decompose phase into the in-phase/quadrature components

$$\begin{aligned}\phi_F(t; \mathbf{x}_F) &= \Re \left\{ \sum_{n=1}^N \alpha_{F,n} \exp(j\omega_n t) \right\} \\ &= \sum_{n=1}^N \Re\{\alpha_{F,n}\} \cos(\omega_n t) + \Im\{\alpha_{F,n}\} \sin(\omega_n t) \quad (16) \\ &= \sum_{n=1}^N \alpha_{F_r,n} \cos(\omega_n t) + \alpha_{F_i,n} \sin(\omega_n t),\end{aligned}$$

where $\Re\{\cdot\}$ extracts the real part of the argument. The Fourier-based parameters are actually comprised of the $2N$ real elements $\mathbf{x}_F = [\mathbf{x}_{F_r}^T \ \mathbf{x}_{F_i}^T]^T$ in which $\mathbf{x}_{F_r} = [\alpha_{F_r,1} \ \alpha_{F_r,2} \ \dots \ \alpha_{F_r,N}]^T$ and $\mathbf{x}_{F_i} = [\alpha_{F_i,1} \ \alpha_{F_i,2} \ \dots \ \alpha_{F_i,N}]^T$ scale the $2N$ quasi-basis functions in the last line of (16). It was shown in [12] via the Jacobi-Anger expansion and after invoking the Central Limit Theorem that the Fourier quasi-basis produces a Gaussian-shaped spectral density in the expectation over a random symbol constellation.

The $2N$ quasi-basis functions in (16) can be easily discretized by sampling the constituent $\cos(\cdot)$ and $\sin(\cdot)$ terms, again noting the need to oversample as before, thereby realizing $\mathbf{b}_{C,n}$ and $\mathbf{b}_{S,n}$, respectively. Consequently, we can construct a discretized representation similar to (2) and (15) via

$$\mathbf{s}_F = \exp(j\mathbf{B}_F \mathbf{x}_F) \quad (17)$$

where the $M \times 2N$ quasi-basis matrix $\mathbf{B}_F = [\mathbf{B}_C \ \mathbf{B}_S]$ consists of $\mathbf{B}_C = [\mathbf{b}_{C,1} \ \dots \ \mathbf{b}_{C,N}]$ and $\mathbf{B}_S = [\mathbf{b}_{S,1} \ \dots \ \mathbf{b}_{S,N}]$. To provide a fair comparison in terms of degrees-of-freedom, in the results to follow we shall set N to be half that used for the other cases.

V. SIMULATION RESULTS

It was observed in [8] that using a physically meaningful waveform implementation like PCFM (or CE-OFDM here) can provide an optimized FM signal that is inherently constant amplitude and may have good spectral containment, both of which are necessary in practice. Of course, the use of such an implementation does not, by itself, actually guarantee that spectral containment is achieved because that depends on the actual parameters. Indeed, it was shown in [8] that a completely random parameter initialization that does not account for spectral containment tends to preserve the ensuing poor containment after optimization. Conversely, good containment initially likewise tends to be preserved. This tendency is largely due to the p -norm cost-function being highly nonconvex and thus is inclined to achieve local optimality (i.e. refines the given initialization), which is actually desirable from the perspective of producing unique waveforms (if also well-contained).

At minimum, it is therefore necessary to either *a*) provide an initial parameterization that is spectrally well-contained, *b*) impose a suitable containment constraint on the optimization, or *c*) employ a cost function that inherently addresses spectral containment (e.g. [21-23]). One could also employ some

combination of these. Here we rely on proper initialization so that the optimization reviewed in Sect. II can be applied without modification, since our goal is to compare these quasi-bases.

Because an arbitrary random instantiation would not possess good containment, we initialize with an independent set of pseudo-random optimized (PRO) FM waveforms [22] that have already undergone spectral shaping via an alternating (time/frequency) projections procedure. Specifically, $K = 3000$ unique waveforms having time-bandwidth product $TB = 200$ and $4\times$ oversampling (relative to 3-dB bandwidth) were first generated using a super-Gaussian (SG) spectral template with shape parameter of 8 [24,25]. At one extreme, an SG parameter of 2 yields a regular Gaussian spectral density and at the other extreme the spectral density becomes rectangular as the SG parameter approaches ∞ . Denoting the resulting discretized phase of the k th PRO-FM waveform as $\phi_{k,0}$, it is set equal to \mathbf{B}_x from (2), $\mathbf{B}_2 \tilde{\mathbf{x}}_2$ from (15), or $\mathbf{B}_F \mathbf{x}_F$ from (17). A simple least-squares estimate is subsequently obtained for each parameter vector to realize a suitable mapping for initialization.

Gradient-descent optimization via [8] (Sect. II) was then performed using a norm value of $p = 8$ for each waveform according to each of the three quasi-bases. Fig. 1 illustrates representative convergence for a single random waveform instantiation that typifies each set. Noting that the initial waveforms had already been optimized, though the least-squares mapping above would certainly introduce degradation, roughly 10 dB reduction in the cost function is observed for the 1st order PCFM and Fourier cases. While optimization of all three cases yields improvement, the 2nd order PCFM case is clearly converging much slower and is still ongoing.

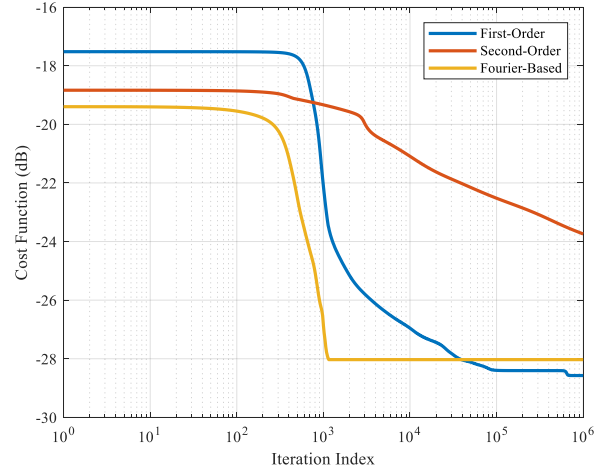


Fig. 1: GISL cost function convergence for 1st order PCFM, 2nd order PCFM, and Fourier quasi-bases over 10^6 gradient-descent iterations for $p = 8$

Figs. 2 and 3 show the associated autocorrelation responses based on root-mean-square (RMS) average or coherent combining (i.e. slow-time processing) of the 3000 unique autocorrelations in each case. Interestingly enough, despite the converged results in Fig. 1 for the 1st order and Fourier cases (with the former being slightly better), the RMS results show a roughly 2 dB lower sidelobe level for the latter (ignoring “shoulder” lobes). Moreover, the reason for slower 2nd order convergence is now understood to be linked to the higher

shoulder lobes visible in Fig. 3 that are inherited from PRO-FM initialization using the super-Gaussian design template, suggesting the optimization for this quasi-basis gets stuck in local minima across the whole set of 3000 unique waveforms.

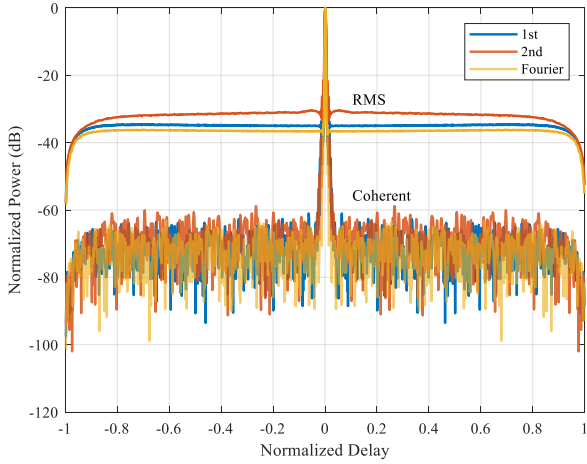


Fig. 2: RMS and coherent combination of autocorrelations for 3000 unique waveform optimized for 1st and 2nd order PCFM and Fourier quasi-bases

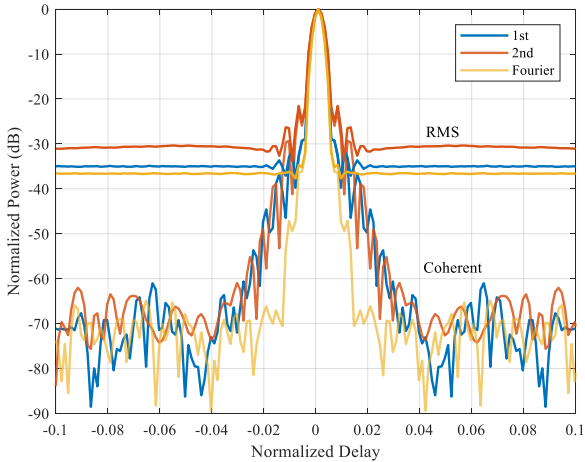


Fig. 3: RMS and coherent combination of autocorrelations for 3000 unique waveform optimized for 1st and 2nd order PCFM and Fourier quasi-bases (mainlobe close-up)

The cause for different sidelobe levels across quasi-bases becomes more apparent when examining the spectral densities in Figs. 4-6, each of which is also a result of averaging across the 3000 optimized waveforms for the given quasi-basis. For instance, the 2nd order spectral density (Fig. 5) clearly has better overall containment than both the PRO-FM initialization and 1st order (Fig. 4), especially at the roll-off edges. Moreover, 2nd order achieves stricter passband containment than 1st order, almost exactly following the tight roll-off from 3 dB down to 10 dB. In contrast, the Fourier quasi-basis (Fig. 6) has expanded to conform to the usual random CE-OFDM response of a Gaussian spectral density [12], which readily explains the lower sidelobe response (a Gaussian spectral density yields a Gaussian autocorrelation). Of course, this more gradual spectral density necessitates higher oversampling of the discretized waveform representation in order to limit transmitter distortion, which can be prohibitive for wideband systems.

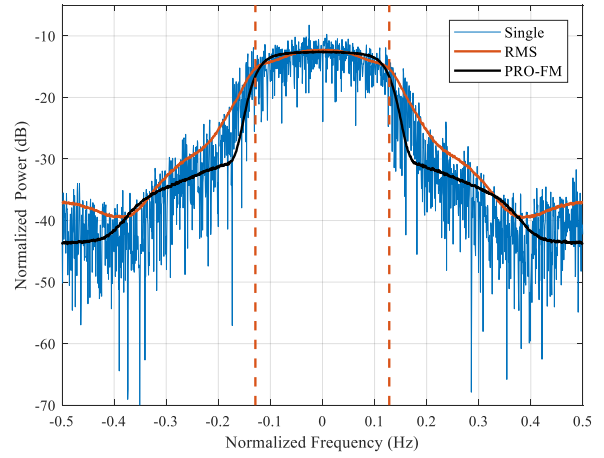


Fig. 4: Average spectral density over 3000 waveforms optimized using $p = 8$ norm for 1st order PCFM quasi-basis

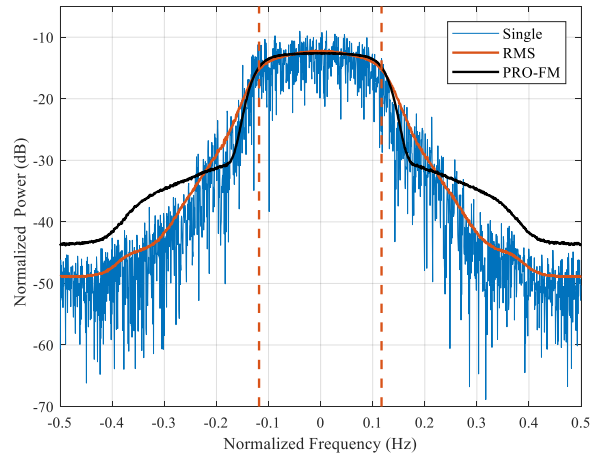


Fig. 5: Average spectral density over 3000 waveforms optimized using $p = 8$ norm for 2nd order PCFM quasi-basis

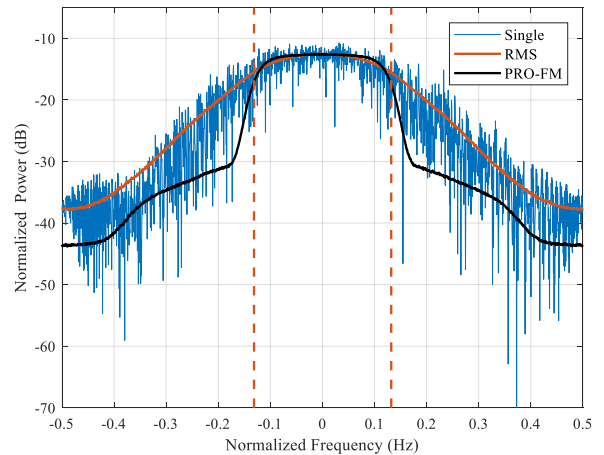


Fig. 6: Average spectral density over 3000 waveforms optimized using $p = 8$ norm for Fourier quasi-basis

It is also instructive to consider examples of instantaneous phase and frequency for each quasi-basis class, as depicted in Figs. 7 and 8, respectively, along with the particular PRO-FM initialization. As expected, since all cases are FM waveforms, the instantaneous phase of each is continuous in Fig. 7. Moreover, 1st order PCFM exhibits a piece-wise linear phase

trajectory, while PRO-FM, 2nd order, and Fourier clearly have a smoother undulating behavior.

The instantaneous frequency plot in Fig. 8 is obtained by taking the sample-to-sample difference of the individual discretized phase functions in Fig. 7. We see that 1st order has discontinuities interspersed with flat frequency regions, which directly arises from (1) and (3) given the use of a rectangular shaping filter. Moreover, since the 2nd order case also uses a rectangular shaping filter (albeit in the 2nd derivative, or chirp-rate, domain), it exhibits piece-wise linear instantaneous frequency. The infinitely differentiable nature of the Fourier quasi-basis reveals a smooth frequency structure as expected, though the span of frequency excursions are notably larger, which likewise explains the expanded roll-off above. We also see that the PRO-FM initialization has an instantaneous frequency that is a bit more jagged than the rest, owing to the fact that it is designed in a discretized manner that has no connection to a spectrally contained **B** structure (hence the need for alternating projection onto a desired spectral template [21]).

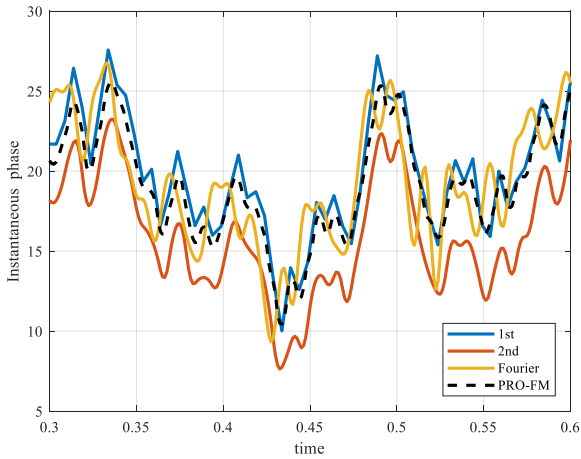


Fig. 7: Close-up section of instantaneous phase of a single waveform optimized for 1st and 2nd order PCFM and Fourier quasi-bases, with PRO-FM initialization

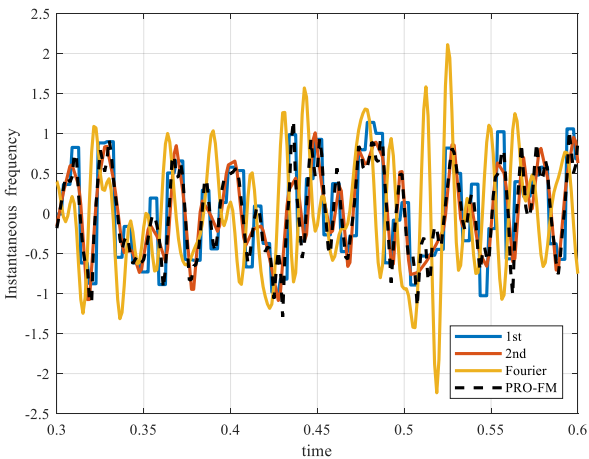


Fig. 8: Close-up section of instantaneous frequency of a single waveform optimized for 1st and 2nd order PCFM and Fourier quasi-bases, with PRO-FM initialization

VI. EXPERIMENTAL RESULTS

Finally, Figs. 9-11 illustrate open-air measurements made at the University of Kansas using each set of nonrepeating waveforms, collected at a center frequency of 3.45 GHz and pulse repetition interval (PRI) of 22 μ s. Simple projection-based clutter cancellation was performed along with -35 dB Taylor windowing in Doppler. The waveform sets were interleaved so that the illuminated scene is almost exactly the same across the three cases.

The main point of these results is to emphasize that, despite their different quasi-basis structures, all three cases yield physically realizable waveforms that are amenable to hardware. The only real difference, which is only barely discernible from visual inspection, is a 2 dB higher background floor for the 2nd order case compared to 1st order or Fourier, which is directly attributable to the higher sidelobe response in Figs. 2 and 3 due to incomplete optimization convergence for the 2nd order case. However, this level is also still quite low as a result of incoherent sidelobe averaging when performing slow-time (Doppler) processing that provides roughly $10 \log_{10}(3000) = 35$ dB of additional suppression (mainlobes remain coherent).

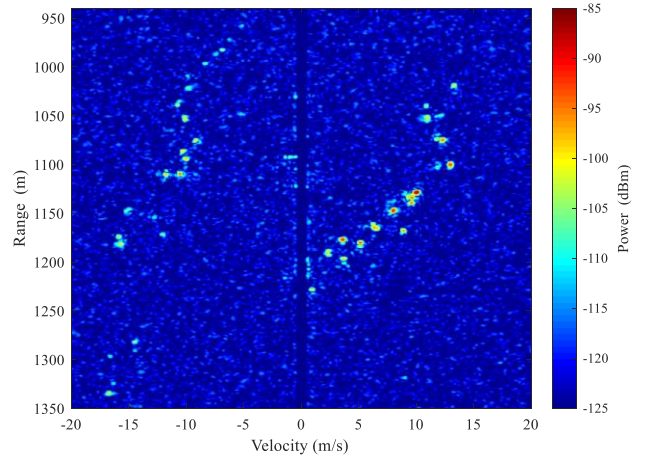


Fig. 9: Open-air range-Doppler response after simple clutter cancellation using 3000 unique 1st order PCFM optimized waveforms

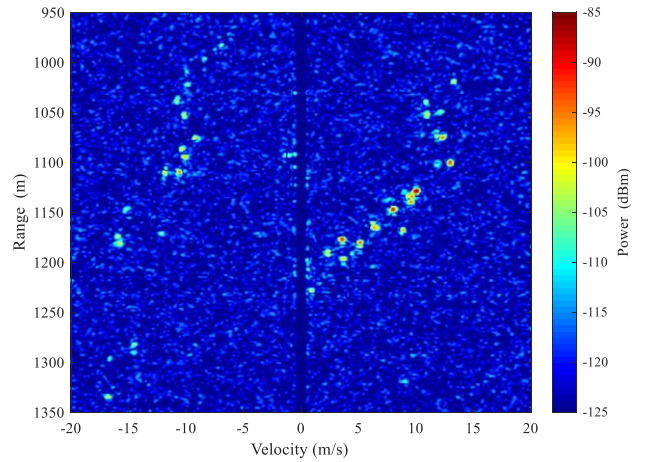


Fig. 10: Open-air range-Doppler response after simple clutter cancellation using 3000 unique 2nd order PCFM optimized waveforms

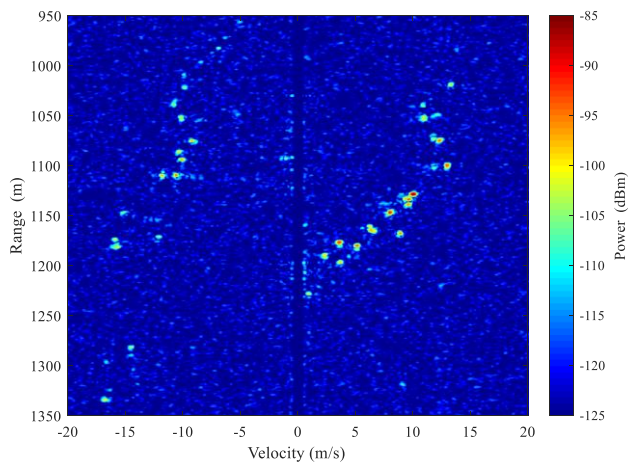


Fig. 11: Open-air range-Doppler response after simple clutter cancellation using 3000 unique Fourier optimized waveforms

VII. CONCLUSIONS

Leveraging a recent p -norm based gradient-descent method for optimizing parameterized FM waveforms, the impact of selecting different quasi-bases for this parameterization was examined. A given quasi-basis must be oversampled so that out-of-band spectral roll-off is appropriately captured, itself a requirement to limit transmitter distortion when a given waveform is implemented in hardware. Consequently, different quasi-bases represent different regions of the infinite space of possible FM waveforms and can therefore possess distinct attributes. Here, 1st and 2nd order PCFM and Fourier structures were evaluated, from which were observed different spectral containment, range sidelobe, phase/frequency smoothness, and optimization convergence characteristics. Combined with the variety of potential initializations (and other quasi-bases), meaningful spectral constraints that could be applied, and other prospective optimization procedures, along with the general non-convex nature of the problem, the overall implication is a vast array of possible waveform types that could be obtained.

REFERENCES

- [1] S.D. Blunt, E.L. Mokole, "An overview of radar waveform diversity," *IEEE Aerospace & Electronic Systems Mag.*, vol. 31, no. 11, pp. 2-42, Nov. 2016.
- [2] B.M. Horton, "Noise-modulated distance measuring systems," *Proc. IRE*, vol. 47, no. 5, pp. 821-828, May 1959.
- [3] S.R.J. Axelsson, "Random noise radar/sodar with ultrawideband waveforms," *IEEE Trans. Geoscience & Remote Sensing*, vol. 45, no. 5, pp. 1099-1114, May 2007.
- [4] T.B. Whiteley, D.J. Adrian, "Random FM autocorrelation fuze system," U.S. Patent #4,220,952, issued 2 Sept. 1980, filed 17 Feb. 1956.
- [5] S.R.J. Axelsson, "Noise radar using random phase and frequency modulation," *IEEE Trans. Geoscience & Remote Sensing*, vol. 42, no. 11, pp. 2370-2384, Nov. 2004.
- [6] L. Pralon, B. Pompeo, J.M. Fortes, "Stochastic analysis of random frequency modulated waveforms for noise radar systems," *IEEE Trans. Aerospace & Electronic Systems*, vol. 51, no. 2, pp. 1447-1461, Apr. 2015.
- [7] S.D. Blunt, et al., "Principles & applications of random FM radar waveform design," *IEEE Aerospace & Electronic Systems Mag.*, vol. 35, no. 10, pp. 20-28, Oct. 2020.
- [8] C.A. Mohr, P.M. McCormick, C.A. Topliff, S.D. Blunt, J.M. Baden, "Gradient-based optimization of PCFM radar waveforms," *IEEE Trans. Aerospace & Electronic Systems*, vol. 57, no. 2, pp. 935-956, Apr. 2021.
- [9] S.D. Blunt, M. Cook, J. Jakabosky, J.D. Graaf, E. Perrins, "Polyphase-coded FM (PCFM) radar waveforms, part I: implementation," *IEEE Trans. AES*, vol. 50, no. 3, pp. 2218-2229, July 2014.
- [10] P.M. McCormick, S.D. Blunt, "Gradient-based coded-FM waveform design using Legendre polynomials," *IET Intl. Conf. Radar Systems*, Belfast, UK, Oct. 2017.
- [11] P.S. Tan, J. Jakabosky, J. Stiles, S. Blunt, "Higher-order implementations of polyphase-coded FM radar waveforms," *IEEE Trans. Aerospace & Electronic Systems*, vol. 55, no. 6, pp. 2850-2870, Dec. 2019.
- [12] S.C. Thompson, A.U. Ahmed, J.G. Proakis, J.R. Zeidler, "Constant envelope OFDM phase modulation: spectral containment signal space properties and performance," *IEEE Military Communications Conf.*, Monterey, CA, Oct./Nov. 2004.
- [13] S.C. Thompson, J.P. Stralka, "Constant envelope OFDM for power-efficient radar and data communications," *Intl. Waveform Diversity & Design Conf.*, Kissimmee, FL, Feb. 2009.
- [14] E.R. Biehl, C.A. Mohr, B. Ravenscroft, S.D. Blunt, "Assessment of constant envelope OFDM as a class of random FM radar waveforms," *IEEE Radar Conf.*, Florence, Italy, Sept. 2020.
- [15] D.A. Hague, "Adaptive transmit waveform design using multitone sinusoidal frequency modulation," *IEEE Trans. Aerospace & Electronic Systems*, vol. 57, no. 2, pp. 1274-1287, April 2021.
- [16] D.G. Felton, D.A. Hague, "Characterizing the ambiguity function of the constant-envelope OFDM waveforms," *IEEE Radar Conf.*, San Antonio, TX, May 2023.
- [17] T.J. Kramer, E.R. Biehl, M.B. Heintzelman, S.D. Blunt, E.D. Steinbach, "Compact parameterization of nonrepeating FMCW waveforms," *IEEE Radar Conf.*, San Antonio, TX, May 2023.
- [18] E. Ghadimi, R. Feyzmahdavian, M. Johansson, "Global convergence of the heavy-ball method for convex optimization," *European Control Conf.*, Linz, Austria, July 2015.
- [19] J.B. Anderson, T. Aulin, C. Sundberg, *Digital Phase Modulation*. Plenum Press, 1986.
- [20] D.G. Felton, D.A. Hague, "Gradient-based optimization of constant envelope OFDM waveforms," *IEEE Radar Conf.*, San Antonio, TX, May 2023.
- [21] S.D. Blunt, J. Jakabosky, M. Cook, J. Stiles, S. Seguin, E.L. Mokole, "Polyphase-coded FM (PCFM) radar waveforms, part II: optimization," *IEEE Trans. AES*, vol. 50, no. 3, pp. 2230-2241, July 2014.
- [22] J. Jakabosky, S.D. Blunt, B. Himed, "Spectral-shape optimized FM noise radar for pulse agility," *IEEE Radar Conf.*, Philadelphia, PA, May 2016.
- [23] C.A. Mohr, P.M. McCormick, S.D. Blunt, C. Mott, "Spectrally-efficient FM noise radar waveforms optimized in the logarithmic domain," *IEEE Radar Conf.*, Oklahoma City, OK, Apr. 2018.
- [24] C.A. Mohr, S.D. Blunt, "Designing random FM radar waveforms with compact spectrum," *IEEE Intl. Conf. Acoustics, Speech & Signal Processing*, Toronto, Canada, June 2021.
- [25] M.B. Heintzelman, T.J. Kramer, S.D. Blunt, "Experimental evaluation of super-Gaussian-shaped random FM waveforms," *IEEE Radar Conf.*, New York City, NY, Mar. 2022.